Ecological Modelling 264 (2013) 7–16

Contents lists available at SciVerse ScienceDirect

Ecological Modelling

journal homepage: www.elsevier.com/locate/ecolmodel

Modeling suspended solids in a Northern Chilean Patagonia glacier-fed fjord: GLOF scenarios under climate change conditions

Víctor H. Marín[a,*], Antonio Tironi[a], María Alejandra Paredes[a], Manuel Contreras[b]

[a] Laboratorio de Modelación Ecológica, Departamento de Ciencias Ecológicas, Facultad de Ciencias, Universidad de Chile, Casilla 653, Santiago, Chile
[b] Centro de Ecología Aplicada Ltda., Suecia 3307, Santiago, Chile

ARTICLE INFO

Article history:
Available online 7 July 2012

Keywords:
Chilean fjords
Climate change
GLOFs
Suspended solids
Baroclinic model

ABSTRACT

Suspended solids play an ecologically important role in glacier-fed fjords, given its dominant effect on their primary production arising from the generation of turbid water plumes by retreating glaciers, which increase light attenuation. Glacial-lake outburst floods, GLOFs, are sudden releases of lake-water impounded by a glacier which may affect either locally or regionally depending on the amount of water and suspended solids released. Chilean Patagonia has been characterized by some of the fastest glacial retreats worldwide and by an increase in GLOFs events. In this article we describe the development of a hydrodynamic model to study the distribution of suspended solids in the Baker channel, a glacier-fed fjord located in Northern Chilean Patagonia. We further describe the simulation of three climate change induced GLOF scenarios and discuss their potential effects on fjord's primary production. The model was implemented as a two-level, one-way, nested hierarchy using the MOHID water modeling system. The large extent, oceanic, level corresponded to a one-layer barotropic model, while the smaller extent, fjord, level corresponded to a 3D baroclinic model with 31 Cartesian layers. Velocities, salinity and suspended solids concentrations were calibrated using field measurements. Results show that the most likely scenario is a decrease in light penetration within the inner fjord's area. Only the most catastrophic scenario, equivalent to a large recorded paleo-discharge, would affect outer areas of the Northern Chilean fjords.

1. Introduction

1.1. Glacial systems, fjords and climate change: the Patagonian fjords

Patagonian fjords and channels, located in southern Chile where the Andes meets the Pacific Ocean, are characterized by a heterogeneous orography, highly stratified estuaries, high-flow steep rivers, high precipitation (annual mean between 1500 and 4500 mm) and by the influence of two of the largest temperate ice bodies of the southern hemisphere: the Northern and Southern Patagonian Ice Fields (Lopez et al., 2010). Watersheds in this region are important contributors of suspended solids, which, in turn, affect the light environment on the fjords and consequently their primary production (see Section 1.2). Suspended solids, also known as glacier flour, are particularly important in glacier-fed fjords such as the Baker channel in southern Chile (Prado-Fiedler, 2009; Vargas et al., 2011). Glacier flour, given its dominant effect on the primary production of coastal waters, arising from the generation of turbid water plumes by retreating glaciers, has been particularly analyzed in relation to glacier melting and global climate change in other regions of the planet (e.g. Zajączkowski and Wlodarska-Kowalczuk, 2007; Barron and Barron, 2005). Furthermore, transport and distribution of suspended solids have been identified as key processes in the management of estuarine coastal systems (Mitchell et al., 2008).

Although the effects of climate change on glacier-fed river discharges are still under discussion, some general patterns are emerging. In a warmer climate the current melting–freezing equilibrium of glaciers will be altered, resulting in potential overall melting. In the long term, considering an average dynamics, this means a rise in river discharges up to a maximum, followed by a decrease until the glacier disappears (McCarthy et al., 2001). However, other short-term, catastrophic, events must also be considered. Glacial-lake outburst floods, GLOFs (or 'jokulhlaups' in Icelandic), are sudden releases of lake-water impounded by a glacier, with effects from local to regional scales depending on the amount of water released. In terms of water discharges, GLOFs in Iceland, Norway, Kyrgyzstan and Chile have shown peak waterflows up to 2–6 times base-flows. If analyzed in terms of suspended solid (SS) discharges, they show 8-fold increases in SS concentration and up to 20 times increases in SS transport. In one case study in Iceland, a series of GLOFs, in a 20-day period, accounted for 19% and 50% of the annual budget of both water and SS discharges

* Corresponding author. Tel.: +56 2 2712978; fax: +56 2 2727363.
E-mail address: vmarin@antar.uchile.cl (V.H. Marín).

0304-3800/$ – see front matter © 2012 Elsevier B.V. All rights reserved.
http://dx.doi.org/10.1016/j.ecolmodel.2012.06.017

Table 1
Type of glacial-lake dams and outburst causes (based on Ghimire, 2005).

Dam type	Outburst cause
Ice	Ice melts glacier retreats Tunnel under ice Over topping by glacier calving, ice fall or rock
Moraine	Piping Over topping by glacier calving, ice fall or rock
Ice-core moraine	Ice core melts resulting in piping Over topping by glacier calving, ice fall or rock

respectively (Dussaillant et al., 2009; Old et al., 2005; Ng et al., 2007; Clarke et al., 2003).

There are various kinds of GLOFs, depending on the nature of the barrier forming the glacial-lake and how that barrier, either ice or a moraine is surpassed, provoking the outburst (Ghimire, 2005). For each kind of lake, a series of outburst causes exist which are summarized in Table 1. In the case of Patagonian Ice Fields, the most common type of GLOF, all of them registered in the Cachet 2 Lake in the Northern Patagonian Ice Field, have corresponded to an ice dammed glacial-lake with a tunnel acting as drainage (see Section 2.1 for more details).

1.2. Phytoplankton dynamics in the Chilean fjords: the effects of the light environment

Light is an environmental variable that regulates the structure and dynamics of phytoplankton (Reynolds, 1997). Its availability to photosynthetic cells is related to turbulence (Margalef, 1978), that allows them to remain in the euphotic zone above their compensation depth (Huisman et al., 1999) and to its attenuation due to dissolved substances, suspended solids and phytoplankton itself (Kirk, 1994). Glacier melting areas can be characterized by their high suspended solid and organic matter content (Pickard, 1971), which increase light attenuation and decrease local primary production (Montecino and Pizarro, 2008; Pizarro et al., 2005).

The available literature shows that glacial melting areas within the Chilean fjords, such as the one modeled in this article (see Section 2.1), correspond to low primary production systems due to their high suspended solid concentration (Aracena et al., 2011; González et al., 2011; Montecino and Pizarro, 2008; Silva and Guzmán, 2006). Further away from glacial melting areas, primary production seems to be regulated by other variables such as nutrients and cell size (Iriarte et al., 2007; González et al., 2011; Paredes and Montecino, 2011).

Chilean Patagonia has been characterized by some of the fastest glacial retreats in the world (Boyd et al., 2008; Lopez et al., 2010) and by an increase in GLOF events, six times in the past two years (Casassa et al., 2010). Thus, it is imperative to analyze the potential effects that such retreats may have on local marine ecosystems especially in the face of global warming. In this article we describe the development of a hydrodynamic model to study the distribution of suspended solids in a glacier-fed fjord, the Baker channel system, in Northern Chilean Patagonia. We describe the simulation of three climate change induced GLOF scenarios and discuss their potential effects on fjord's primary production.

2. Model development

2.1. The Baker channel fjord system

The Baker channel is a glacier-fed fjord located at 48°S in Chilean Patagonia (Figs. 1 and 2). Its main sources of fresh water are the Baker and Pascua Rivers, which have been identified as containing Chile's remaining hydroelectric potential (Vargas et al., 2011; HydroAysén, 2010). Their watersheds are also known for various

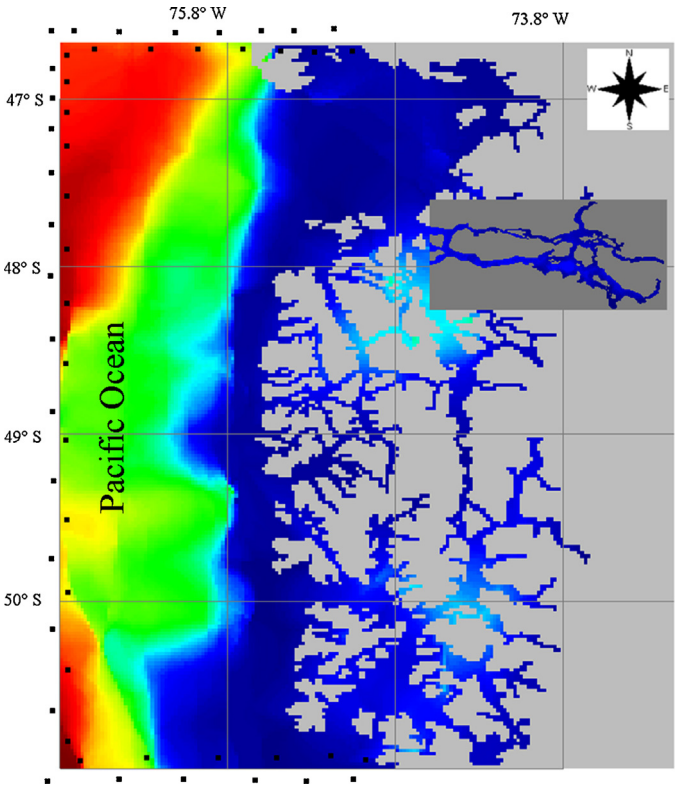

Fig. 1. Geographic limits of the modeling area. The larger area corresponds to the oceanic grid, black squares in the oceanic border represent the locations where the boundary condition (FES2004 tide) was imposed. The smaller, gray, area corresponds to the fjords grid.

GLOF events in the last couple of years. On the upper part of the Baker watershed, within the Northern Patagonian Ice Field, the Cachet 2 Lake, with an area of 4 km^2, has already shown six GLOF events in the last two years. In this case, the Colonia glacier has acted as an ice dam for the lake and an 8 km long tunnel as the drainage to each flood, caused by the weakening of the ice dam due to the long term thinning of the glacier (Casassa et al., 2010). As an example, Fig. 3 shows a hydrograph for the last couple of GLOF events registered during the first quarter of 2012. Thus, river flows during a GLOF increase, under current climate, at least double its normal value. Indeed, during the event of 2009 the flow of the Baker River increased from 2000 $m^3\ s^{-1}$ to nearly 6000 $m^3\ s^{-1}$ in few hours[1] (Dussaillant et al., 2009).

The bathymetry of the Baker channel goes from close to 10 m at fjord's head to a maximum of 1250 m in its deepest part, a small zone within the main channel. The fjord communicates with the open ocean through two narrow (5 km and 3.5 km wide) deep channels (close to 250 m) with no shallower sills. We restricted, for modeling purposes, the maximum fjord depth to 500 m (Fig. 2). This restriction only affected two small zones within the modeling area, with not consequences on the overall model performance.

2.2. The MOHID water modeling system

Fjords, from a hydrodynamic point of view, are deep highly stratified estuaries with a shallow (5 m) seaward surface layer. These characteristics represent an important challenge for the development of hydrodynamic 3D baroclinic models, since vertical resolution has to be high enough (e.g. layer widths ≤1 m)

[1] Data available also at: http://www.dga.cl.

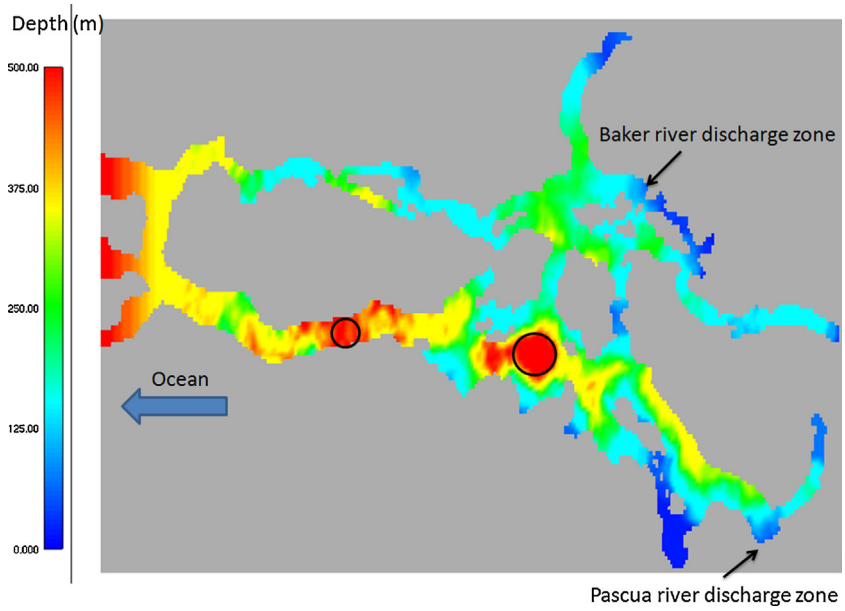

Fig. 2. Bathymetry of the fjords grid. The two circles in the main channel represent areas where bottom was changed to a maximum depth of 500 m.

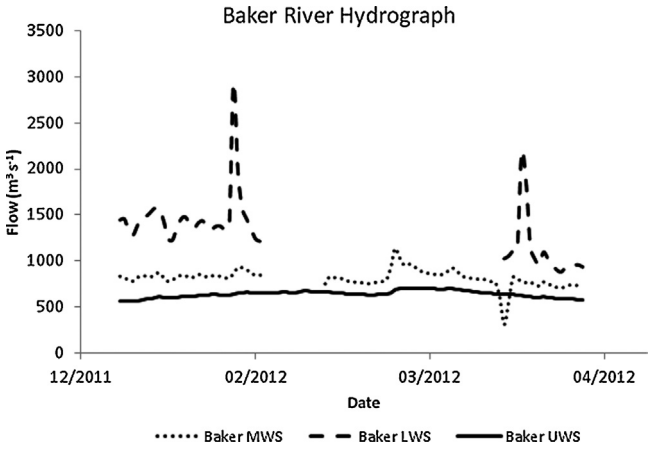

Fig. 3. Hydrograph of the GLOF events occurred at the Baker watershed in the Northern Patagonian Ice Field. UWS, upper watershed station; MWS, middle watershed station; LWS, lower watershed station. Data was obtained from automated hydrological stations from the Chilean Water Directorate (http://www.dga.cl).

to solve the surface layer without compromising model stability. Indeed, there are few numerical, 3D, fjord hydrodynamic models reported in the literature (e.g. Robins and Elliot, 2009; Nyholm et al., 1984; Leonov and Kawase, 2009; Keilegavlen and Bertnsen, 2009; Gustafsson and Bendtsen, 2007).

We have studied and modeled the hydrodynamics and ecology of the Chilean fjords by means of MOHID water modeling system (Campuzano et al., 2008a,b; Marín et al., 2008; Tironi et al., 2010). MOHID[2] is a numerical, freeware, open code system designed to implement three-dimensional models of aquatic ecosystems. It has been developed and it is maintained by scientists from the Marine and Environmental Technology Center (MARETEC; Instituto Superior Técnico; Lisbon Technical University, Portugal). The model description that follows summarizes the information available on MOHID's web page[2]. We have included enough details for the reader to understand the basis of our specific application.

[2] http://www.mohid.com.

MOHID includes a baroclinic hydrodynamic module for the water column, a module for the sediments and corresponding eulerian transport and lagrangian transport modules. The system is composed of pre-processing (MOHID GIS) and post-processing tools (MOHID POST, MOHID Time Series Editor, MOHID Statistical Analyzer) plus a graphical interface for the implementation of models (MOHID GUI). Currently the system is made of more than 40 modules that can be coupled to generate vast applications from marine ecology to oil spills (Neves et al., 2008).

The hydrodynamic module is implemented as finite volumes (Martins et al., 2001). The module solves the three-dimensional incompressible primitive equation assuming hydrostatic equilibrium and using the Boussinesq and Reynolds approximations. The momentum balance equations for mean flow horizontal velocities, in Cartesian form, are:

$$\partial_t u = -d_x(uu) - d_y(uv) - d_z(uw) + fv - \frac{1}{\rho_0}\partial_x p + \partial_x((\nu_H + \nu)\partial_x u) + \partial_y((\nu_H + \nu)\partial_y u) + \partial_z((\nu_v + \nu)\partial_z((\nu_r + \nu)\partial_z u) \quad (1)$$

$$\partial_t v = -d_x(vu) - d_y(vv) - d_z(uw) + fu - \frac{1}{\rho_0}\partial_y p + \partial_x((\nu_H + \nu)\partial_x v) + \partial_y((\nu_H + \nu)\partial_y v) + \partial_z((\nu_v + \nu)\partial_z((\nu_v + \nu)\partial_z v) \quad (2)$$

where u, v and w are the components of the velocity vector in the x, y and z directions respectively, f the Coriolis parameter, ν_H and ν_v the turbulent viscosities in the horizontal and vertical directions, ν the molecular kinematic viscosity and p is pressure. The temporal evolution of velocities is dynamically calculated as the balance of advective transports (first three terms on the right hand side), Coriolis force (fourth term), pressure gradient (next three terms) and turbulent diffusion (last three terms).

The vertical velocity is calculated from the incompressible continuity, mass balance equation:

$$\partial_x u + \partial_y v + \partial_z w = 0 \quad (3)$$

Water properties such as temperature, salinity, sediments and oxygen, among others, are handled by the water properties module, which coordinates their evolution in the water column using a eulerian approach. Their dynamics includes transport due to advective

and diffuse fluxes, water discharges from rivers, sedimentation of particulate matter and internal sinks and sources.

The transport due to advective and diffusive fluxes of a given property A is solved by the following equation:

$$\partial_t A = -\partial_x(vA) - \partial_y(vA) - \partial_x(wA) + \partial_x(\nu'_H \partial_x A) + \partial_y(\nu'_H \partial_y A) + \partial_z((\nu'_v + \nu'_A)\partial_z A) \quad (4)$$

where ν'_H and ν'_v are the horizontal and vertical eddy diffusivities, ν'_A the molecular diffusivity and other terms as previously defined. The first two can be calibrated in MOHID by means of dimensionless factors (SCHMIDT_NUMBER_H for horizontal diffusivity and SCHMIDT_COEF_V for vertical diffusivity) that change the relationship between diffusivity and turbulent viscosity for each property.

Vertical viscosity is calculated by means of the general ocean turbulence model (GOTM[3]), GOTM module under MOHID. The module contains the one-dimensional GOTM water column model designed for marine and limnological applications, containing several alternatives to parameterize vertical turbulence. We tried several schemes with similar results, to finally use the Mellor–Yamada equations.

The turbulence module handles horizontal turbulence. We used the Smagorinsky turbulence model, which is based on the local derivatives and grid size according to the following formula:

$$\nu_L = \Delta x \Delta y \sqrt{\left(\frac{\partial u}{\partial x}\right)^2 + \left(\frac{\partial v}{\partial y}\right)^2 + \frac{1}{2}\left(\frac{\partial u}{\partial x} + \frac{\partial v}{\partial y}\right)^2} \quad (5)$$

This formulation is translated in MOHID as:

$$\nu_H = \text{Horcon} \times \Delta x \times \Delta y \sqrt{\left(\frac{\partial u}{\partial x}\right)^2 + \left(\frac{\partial v}{\partial y}\right)^2 + \frac{1}{2}\left(\frac{\partial u}{\partial x} + \frac{\partial v}{\partial y}\right)^2} \quad (6)$$

where Horcon is a calibration, dimensionless, parameter. We tested other two turbulence schemes (constant and estuary) available in MOHID with lower quality results.

Exchanges between water and the atmosphere are modeled through the surface module, which incorporates water, heat and oxygen fluxes. In our application we included an annual precipitation of 3500 mm. Evaporation was incorporated through latent heat fluxes by means of Dalton's law.

2.3. Sediment and light extinction modeling under MOHID

Sediments within MOHID are modeled as cohesive sediments and managed through three modules: water properties, bottom and free vertical movement. Water properties module manages water column advective and diffusive fluxes, as governed by Eq. (4). The bottom module is responsible for computing fluxes at the water–sediment interface, managing boundary conditions to both water column and sediment column properties. It considered both deposition and erosion using Partheniades (1965) approach.

If the Boolean keyword "vertical_movement" is set to 1 in the water properties module for cohesive sediments, the free vertical movement module is activated for this property. The later is then used to add a vertical movement to the vertical flow and to compute deposition. In our model we imposed a constant, prescribed, settling velocity of 8.5×10^{-5} m s^{-1}, for salinities $\geq$3 PSU and zero otherwise, based on field data on the average particle size of the sediments from the main rivers (between 15 and 70 μm) and settling velocity experiments (Aysen_SEIA, 2012).

[3] http://www.gotm.net.

Sediments in the water column, modeled as described above, were then used to compute light extinction. Since our main objective was to assess the effects that sediments generated from GLOFs would have on the light environment of the fjord, we modeled light extinction as affected by sediment concentration only. MOHID has two ways to model light extinction: Parsons et al. (1984) equation for chlorophyll and Portela (1996) equation for sediments. For the purposes of this model we used Portela's equation, where light extinction coefficient, k, is a function of the concentration of suspended sediments:

$$k = 1.24 + 0.036 C_{ss} \quad (7)$$

where C_{ss} is the concentration of suspended sediments.

2.4. Nested modeling

MOHID can be used to model coastal and estuarine areas of complex bathymetry and topography through one-way nesting (Braunschweig et al., 2004). In nested modeling a medium to large extent, low resolution, hydrodynamic model is used to generate boundary conditions for a second, smaller extent, higher resolution model contained within the geographic boundaries of the first. MOHID, from the perspective of software development, does not have limitations on the number of nesting levels being only limited by RAM size and processor speed. However, practical experience shows that three levels are enough for most applications. In this specific case, we used two nesting levels (Fig. 1). Grids were generated using the "Create Digital Terrain" tool of MOHID GIS. This tool generates numerical grids by means of spatial triangulation using the available bathymetry data. When data is too dispersed, as it was in this case, this tool allows filling no-data areas with the average value of adjacent cells by means of a user-defined radius. We used this technique for both grids, with a 10-cell radius for the first level and a 2-cell radius for the second, smaller extent, level. They were then manually examined in order to correct areas that could generate numerical instabilities (e.g. isolated cells and cells connected only through vertices).

The first level, or oceanic model, was implemented to generate the oceanic boundary conditions corresponding to the astronomical tide. The model was built with a resolution of 0.02° (2.2 km), with its origin at 76.8°W and 50.99°S and with a grid size of 217 (lat.) × 183 (long.). Coastline was obtained from the US NGDC open database (available at: http://www.ngdc.noaa.gov/mgg/shorelines/shorelines.html); bathymetry was obtained from track lines available at GEODAS (http://www.ngdc.noaa.gov/mgg/geodas/trackline.html). The tidal signal was extracted from the FES2004 global tide model (Lyard et al., 2006). Marín and Campuzano (2008) have already shown that the later model generates tidal levels inside the Chilean fjords area (from 41°S to 46°S) consistent with field measurements. Tidal components, 14 in total, were extracted from the FES2004 model by means of the MOHID-tide utility program for 50 boundary points of the oceanic model (Fig. 1).

The second level, or fjord model, corresponded to the area of interest (the Baker channel fjord system; Figs. 1 and 2). All simulations described in this article were implemented on this level. The fjord model was built with a resolution of 0.005° (0.3 km), with its origin at 74.6°W and 48.25°S and with a grid size of 132 (lat.) × 283 (long.). Coastline and bathymetry was obtained from charts available from the Chilean Navy (http://www.shoa.cl). The fjord model takes the tidal signal from the oceanic model at the oceanic boundary between them and includes discharges of continental water fluxes. Both models did not differ in bottom depth at the boundary between them.

Table 2
Width (in meters) of the 31 Cartesian vertical layers of the fjords model. Layer numbering starts from the bottom up to the surface.

Layers	1–6	7–13	14–20	21–31
Width (m)	50	25	2	1

2.5. Vertical structure, boundary and initial condition

The oceanic model was implemented as a barotropic one-layer model, with a constant horizontal viscosity of 100 $m^2\ s^{-1}$. MOHID uses a finite volume approach to discretize equations (Chippada et al., 1998). The procedure for solving them is independent of cell geometry and as volumes can vary in the course of calculus, geometry is updated in every time step.

Vertical coordinates of a hydrodynamic model under MOHID can be built in three ways: sigma-coordinates, Cartesian coordinates or a mixture of both. We tried all three schemes for the fjord model, to finally use Cartesian coordinates (Table 2) due to numerical instabilities generated in both full sigma and sigma-Cartesian versions. Layer thickness decreases from the bottom (50 m) to the surface (1 m) to allow for the resolution of the narrow surface layer. Indeed, surface layer thickness represents a compromise between vertical resolution and numerical stability.

River flows, among the many variables and parameters of the model, were largely those with the highest uncertainties. Baker and Pascua River flows were obtained from the automatic stations of the General Water Directorate of the Chilean Government (http://dgasatel.moptt.cl/index.asp). However, early work conducted within scientists of the HydroAysén project (HydroAysén, 2010) showed that measured values had to be adjusted using a 1.5 factor in order to use them as fjord's discharges, given the location of the automated stations. We modeled the system using river flows for the autumn season of the Southern Hemisphere (April–May). The overall mean value was 2080 $m^3\ s^{-1}$ for the Baker River and 2000 $m^3\ s^{-1}$ for the Pascua River. We further included other three smaller discharges (<60 $m^3\ s^{-1}$ each) within the fjord model using the available information on the Chilean Government Environmental Impact website (http://seia.sea.gob.cl/).

Temperature in the fjord model was initialized with an isothermal value of 10 °C. Salinity, on the other hand, was initialized with different values for each layer (Table 2) according to the following scheme: 0 PSU between the surface and 4 m of depth, followed by a halocline from 1.5 PSU to 32 PSU between 5 m and 50 m; deeper layers were initialized with a 32 PSU value. The data was obtained from the information available at the Chilean Government Environmental Internet System (Aysen_SEIA, 2012).

2.6. Simulation strategy and calibration

Field data on salinity and suspended solids near the discharge zone for both main rivers (Fig. 2) was available from oceanographic campaigns conducted during February, March and May 2009 by Costasur (2009). Consequently, we adjusted simulation times so the calibrated model and the scenarios were run during May 2009. With that purpose, the nested models were run using the following sequence:

1. The ocean, level-1, model was initialized, running on its own without the fjord model, during three and a half months (from January 1st to April 15th, 2009). This long initialization was necessary because previous modeling experiences on the Chilean fjords (Marín and Campuzano, 2008) had shown that astronomical tides imposed at the oceanic boundary would generate transient, anomalous, tidal levels within the fjords system during an initialization period of nearly two months. This initialization further included a gradual increase of tidal components ("slow-start" keyword for the hydrodynamic module) during a 24-h period. The Δt of the oceanic model was set to 60 s for the whole of the simulations.
2. After that period, the fjord model was switched on and initialized, for April 15th 2009, in its barotropic version for a week in order to stabilize the tide coming from the ocean model. River discharges were also started during this period. The Δt for the barotropic initialization of the fjord model was set to 30 s.
3. Having stabilized velocity and basic properties fields (i.e. temperature, salinity and river discharges), the model was switched to its baroclinic, final simulation version, for April 22nd 2009. For all the rest of the simulations the Δt of the fjord model was switched to 10 s. The first scenario (S1 scenario, see Section 2.7) was simulated 11 days after the baroclinic version of the fjord model was initialized, from May 2nd to May 8th, 2009. The nested (ocean+ fjord) model was by then numerically stable, without anomalous transient responses.
4. Calibration of velocity, salinity and suspended solids was accomplished adjusting the dimensionless parameters introduced in Section 2.2 (e.g. Horcon, SCHMIDT coefficient). During this procedure we also used maximum river discharges for both Baker and Pascua Rivers (6000 $m^3\ s^{-1}$ and 4000 $m^3\ s^{-1}$, respectively) in order to adjust the halocline depth to measured values. We used Costasur (2009) data for calibration. Velocity data was obtained with ADCP current meters, between February 21st 2009 and March 24th 2009 at the Baker River discharge area (Fig. 2), moored at 2 m and 12 m of depth. For the Pascua River discharge area (Fig. 2), velocity data was obtained between March 25th and May 1st 2009 with moored instruments at 2 and 5 m of depth. Salinity vertical profiles, and surface suspended solids were measured on May 2nd through 4th 2009 with a Hydrolab multiparameter DS5 sonde. Salinity was available for both river discharge areas while suspended solids were available only for the Baker discharge area. Model data used during calibration corresponded to the last output of the S1 scenario (see Section 2.7 below), which corresponded to May 8th 2009. In order to compare with the data obtained by Costasur (2009), for calibration purposes, we sampled model variables (velocity, salinity and suspended solids) only at both river discharge areas.
5. Scenarios (see next item) were simulated as a time sequence starting with S1, which corresponded to our baseline condition, at simulation day May 8th, 2009 preceding S2 that in turn preceded S3. Thus, final property fields for S1 corresponded to the initial conditions for S2 and so on.

Table 3
Comparison between concentrations of suspended solids (mg l^{-1}) measured in the Baker River discharge area in May 2009 (Costasur, 2009) and simulated by MOHID for maximum river flow.

Station	Data	Model
E-19	42.1	100.29
E-20	119.0	118.44
E-18	105.0	102.98
Average ± standard dev.	88.67 ± 41.02	107.0 ± 9.6
t-Test	$t = -0.754$, $p = 0.49$	

2.7. GLOF scenarios

We constructed three GLOF scenarios for the discharges Baker and Pascua Rivers (Table 4). Each scenario was run during 7 days with constant river flows and suspended solid concentrations for each river. Results shown in this article correspond to the last time step for day 7 under each scenario.

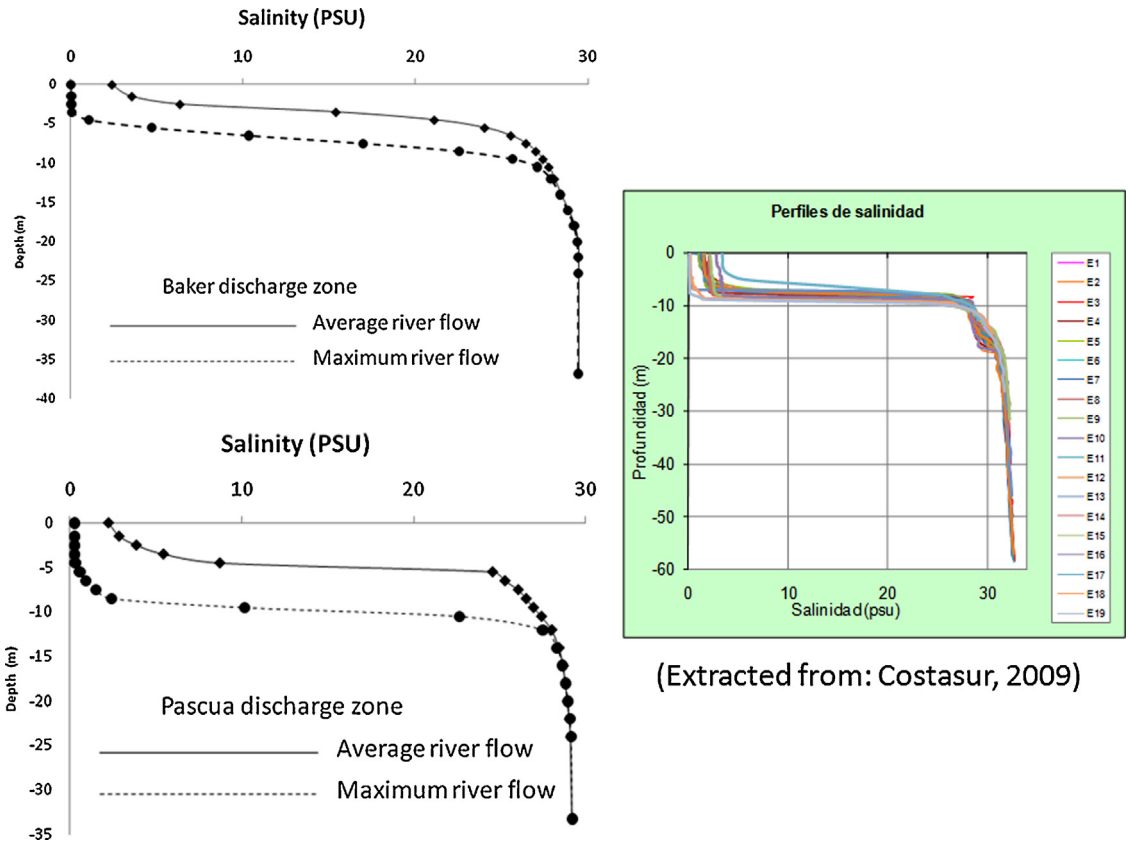

Fig. 4. Vertical distributions of modeled salinity for the Baker and Pascua Rivers discharge zones. The colored figure shows field salinity data obtained by Costasur during May 2009.

2.7.1. S1 scenario (running time: May 2nd–8th, 2009)

A very likely near-future scenario, representing GLOFs like the one that occurred during the summer-fall of 2009 (Dussaillant et al., 2009) with 6000 $m^3\ s^{-1}$ and 4000 $m^3\ s^{-1}$ for the Baker and Pascua Rivers respectively. The model was run with those river flows for one week. Suspended solids concentrations were set to 120 mg l^{-1} (Baker) and 60 mg l^{-1} (Pascua) based on field measurements (Costasur, 2009). Since this was the scenario used for model calibration, we do not include in this article an additional baseline output. Furthermore, as we show in the results section, this scenario represents current conditions for maximum river flows. Smaller flows only showed that suspended solids would affect smaller, inner, areas.

2.7.2. S2 scenario (running time: May 8th–15th, 2009)

Since global warming will, most likely, affect the probability and magnitude of peak discharges in GLOFs (Ng et al., 2007), we prepared a second mid-term climate change scenario assuming a 4.5-fold increase in water discharges up to 9000 $m^3\ s^{-1}$ for the Baker River and 6000 $m^3\ s^{-1}$ for the Pascua River. For suspended solids discharges, we assumed a four-time increase, with 480 mg l^{-1} (Baker) and 240 mg l^{-1} (Pascua). These are moderate values based on measurements for a GLOF in Iceland, which showed a 8-fold increase in SS concentration (Old et al., 2005).

2.7.3. S3 scenario (running time: May 15th–21st, 2009)

Finally, we constructed a catastrophic event, based on estimated values of a modeled "paleo-discharge" (Dussaillant et al., 2009). This run was built assuming a massive discharge of 16,000 $m^3\ s^{-1}$ for the Baker River and 11,000 $m^3\ s^{-1}$ for the Pascua River. For suspended solids we assumed the maximum registered value for contemporary GLOFs, based on the cited literature, with 960 mg l^{-1} (Baker) and 480 mg l^{-1} (Pascua).

Table 4
Climate change simulation scenarios. S1 corresponds to very likely scenario observed during the summer of 2009 that was used to calibrate the model; S2 corresponds to a moderate increase in both water flows and suspended solids (SSs). Finally S3 represents a catastrophic event. See text for further details.

River	Parameter	Scenarios		
		S1	S2	S3
Baker	SS (mg l^{-1})	120	480	960
	Flow ($m^3\ s^{-1}$)	6000	9000	16,000
Pascua	SS (mg l^{-1})	60	240	480
	Flow ($m^3\ s^{-1}$)	4000	6000	11,000

3. Results

3.1. Calibration

The best adjustment between observed and simulated data (see Section 2.6) was obtained with a SCHIMDT_COEF_V = 1.0. Simulations with average river flows produced a shallow (5 m) surface seagoing layer (Fig. 4). Better results were obtained when using maximum river flows. The calibration of velocity profiles showed that the best agreement between measured speeds and simulation results was obtained using a Horcon value (Eq. (6)) equals to 2.5 (Fig. 5). Once again, as shown for salinity, the use of average river flows produced surface currents similar to the average current meter values, but deeper values were consistently slower for the Baker discharge area. The problem was solved using maximum river flows. In the later case, surface velocities approached maximum field values and deeper layer velocities, for the Baker discharge area, were closer to average field values. Finally, the

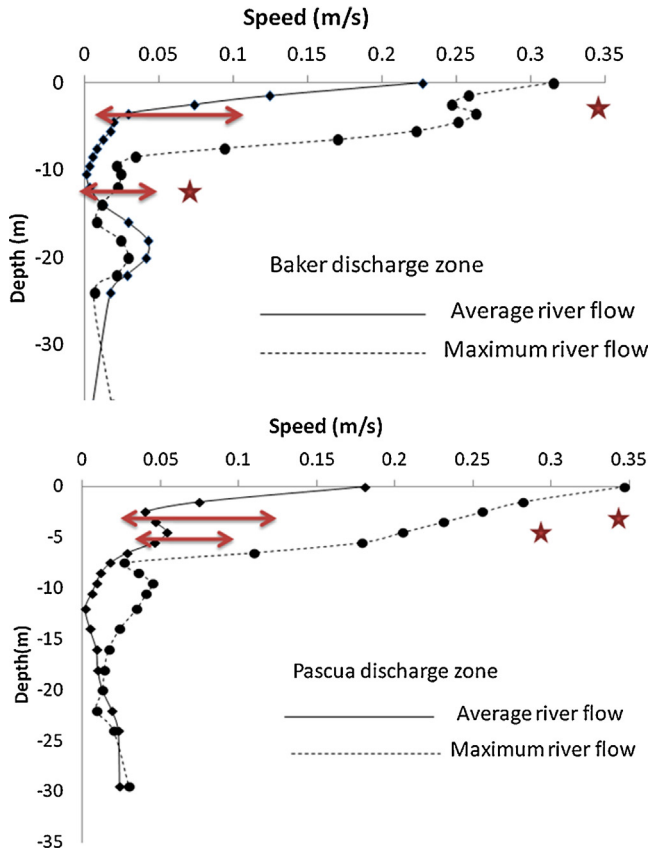

Fig. 5. Vertical distributions of modeled velocity module for the Baker and Pascua Rivers discharge zones. Arrows represent average velocity ± one standard deviation and stars maximum velocity data obtained by Costasur (2009).

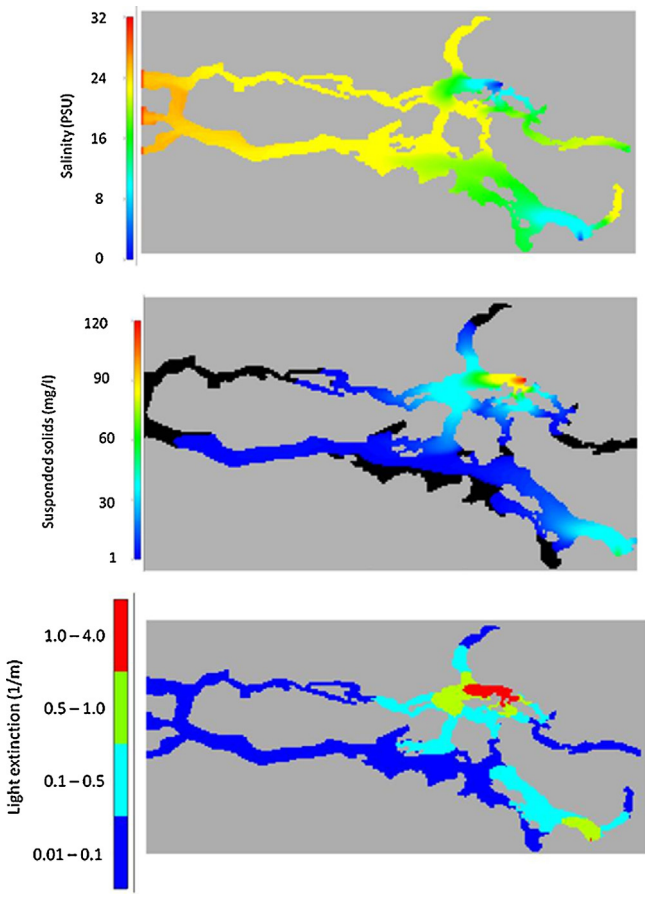

Fig. 6. Model results for surface layer of the S1 scenario (7th-day) for salinity, suspended solid concentration and light extinction.

calibration of suspended solids, based on field data from May 2009 and maximum river values corresponding to the summer 2009 GLOF event, showed not significant differences between modeled and field data (Table 3).

3.2. S1 scenario

Results describing simulations under *S1 scenario* corresponded to the maximum river flows of an observed GLOF event during the summer-fall 2009. The spatial extension of the influence of river flows depended on which variable was considered (Fig. 6). Salinity is influenced all over the model extent reaching values close to 25 PSU and 26 PSU at the ocean border, against an oceanic value of 31 PSU imposed at the oceanic frontier. Suspended solids, on the other hand, decreased from values between 120 mg l^{-1} and 60 mg l^{-1} at fjord's head, near river discharges, to 1.0 mg l^{-1} and 0.5 mg l^{-1} at the oceanic border. Finally, light extinction decreased from values between 1 m^{-1} and 2 m^{-1} at the river discharges sectors to smaller than 0.05 m^{-1} at the oceanic border of the fjord model. Thus, surface suspended solids decreased 240 times from the head to the mouth of the fjord system under the maximum river flow conditions experienced during the 2009 GLOF event.

3.3. S2 and S3 scenarios

Under the *S2 scenario*, most of the fjord's area reached light extinction values higher than 0.5 m^{-1} (Fig. 8), associated with suspended solids in excess of 15 mg l^{-1} (Fig. 7). When the *S3 scenario* was simulated, the bulk of the area showed suspended solids concentration in excess of 30 mg l^{-1} (Fig. 7), generating light extinction values well above 0.5 m^{-1} (Fig. 8). Indeed, for this latter scenario

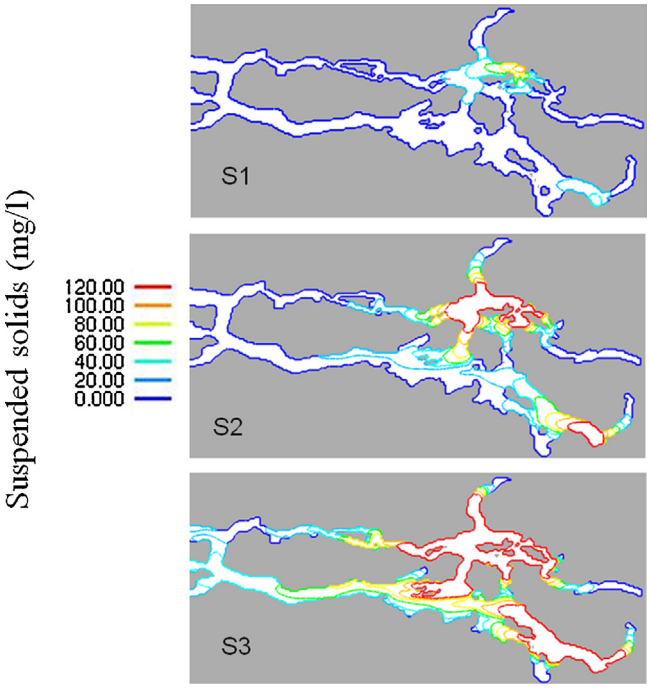

Fig. 7. Comparison of suspended solids model output (surface layer, 7th-day) for S1–S3 scenarios.

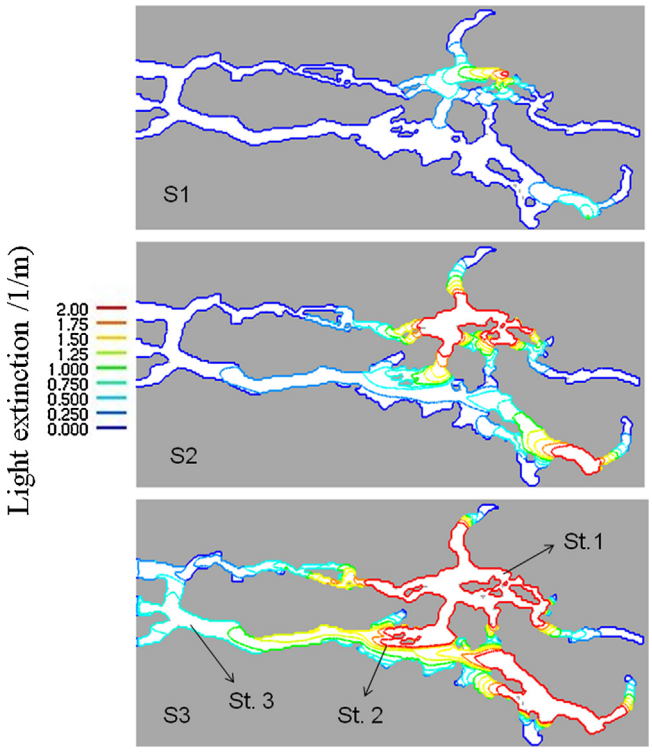

Fig. 8. Comparison of light extinction (surface layer, 7th-day) for S1–S3 scenarios.

light extinction for most of the area was above 1.0 m^{-1}. Nevertheless, the concentration of suspended solids decreased rapidly from the head of the fjord to the oceanic boundary. We compared vertical profiles of suspended solids in three model locations for the S3 scenario (Fig. 9): St. 1 at the Baker River discharge area, St. 2 in the main channel in an intermediate location and St. 3 near the oceanic boundary (see Fig. 8 for specific geographic locations). Although the local Baker River discharge sector receives concentrations near 1000 mg l^{-1} during the S3 GLOF, by the time suspended solids reached the fjord model oceanic boundary they have decreased to 6% of the head value.

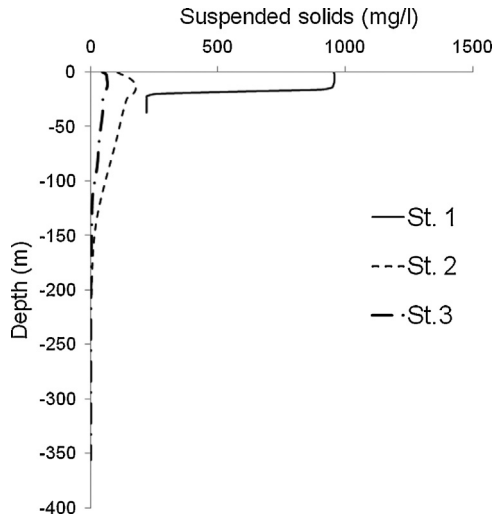

Fig. 9. Vertical distribution of suspended solids, S3 scenario at 7th day, for three model locations (see Fig. 8 for geographic locations).

4. Discussion

There is little doubt that in the near, not too distant, future humanity will have to face the effects of climate change. However, as important as that process shall be, the likely responses of earth ecosystems remain elusive and full of uncertainties. Ecological modeling may play a rather important role generating insights on the physical, ecological and social mechanisms that will govern ecosystems behavior when exposed to such a change (e.g. Marin et al., 2009). In this article we have described a hydrodynamic 3D model designed to study the distribution of suspended solids in a southern Chilean fjord system (the Baker channel fjord located in the Northern Patagonian Ice Field region), including simulations under climate change conditions. The analysis of this region is urgent since it has been identified as one zone with the highest potential for climate change effects (Boyd et al., 2008; Dussaillant et al., 2009). However, modeling the hydrodynamics of fjords, given the strong vertical salinity gradients, requires solving for the surface layers without compromising model's numerical stability. We implemented a 31-layer Cartesian coordinate's model under MOHID water modeling system (Neves et al., 2008). The modeling strategy, with layer width decreasing from the bottom (50 m) to the surface (1 m), produced numerically stable and calibrated hydrodynamic solutions. Furthermore, we have shown that the model can reproduce the effects of a glacial-lake outburst flood (GLOF) recorded during the summer-fall 2009 (Dussaillant et al., 2009). Since GLOFs are one of the likely, and potentially dangerous, non-lineal responses of glacial systems such as the Northern and Southern Ice Fields in Chilean Patagonia, we analyzed the changes in the distribution of terrigenous suspended solids, or glacier flour. Suspended solids are known to have an important influence on glacier-fed fjords primary production (Pizarro et al., 2005). Consequently, we simulated three scenarios: *S1* corresponding to the 2009 GLOF baseline, calibrated, condition, *S2* which simulates a likely GLOF under climate change conditions, observed in other latitudes such as Iceland (Old et al., 2005) and *S3*, a catastrophic paleo GLOF described by Dussaillant et al. (2009). Light and primary production studies in the Chilean fjords show that light extinction coefficients higher than 0.46 m^{-1} (euphotic zones < 10 m) are found in areas where production is severely limited by light (Pizarro et al., 2005). Indeed, these authors postulate a three-phase model describing the relationship between light availability and chlorophyll concentration. Phase A is characterized by euphotic zone depths less than 20 m, where light limitation is related to the input of terrigenous sediments. Results (Figs. 6–9) show that suspended solids at the oceanic border, in 7-day simulations, decreased well below 10% of near-discharge concentrations located nearly 100 km upstream, considering surface seagoing fjord flows. This result, which agrees with sediment data analyzed by Silva et al., 2011 for other northern Chilean fjords, suggests that climate change effects on glacier melting will most likely affect the inner sectors of the Chilean fjords with minor effects on more oceanic areas, unless a catastrophic event such as the *S3 scenario* is considered (Figs. 8 and 9). In that case, suspended solids concentrations at the oceanic frontier of the model reached values higher than 30 mg l^{-1}, with light extinctions coefficients above 0.5 m^{-1}. Such a light environment is likely to seriously affect primary production in the water column at least up to the oceanic frontier of our fjord model.

Thus, our results can be summarized as shown in Fig. 10. Under fluctuations in suspended solid concentrations in Chilean fjords as currently observed, *S1 scenario* and lower, light limitation of primary production is likely to be restricted to inner fjords, mostly those directly influenced by glacier-fed rivers such as the Baker and Pascua (Fig. 6). If climate change increases air temperature and this process, in turn, increases glacier's melting then there are two potential scenarios: slow increase in melting rates reaching *S2*

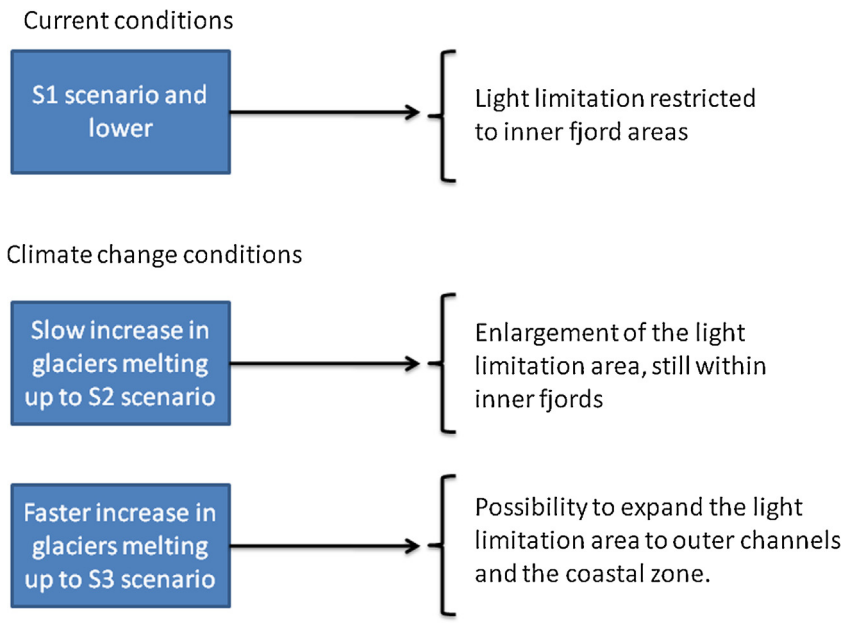

Fig. 10. Summary for the interpretation of S1–S3 scenarios in terms of spatial extension fjord's primary production light limitation.

scenarios (Figs. 7 and 8) or faster and highly non-linear increase generating *S3*, catastrophic, *scenarios*. In the first case (*S2*) we propose that there will be an enlargement of the light limitation areas but still within the inner fjords. Only the later condition (*S3*) is likely to generate a wider low productivity area, potentially reaching outer channels and even coastal waters, due to light limitation by increased terrigenous suspended solids.

Acknowledgments

We thank Kenneth A. Rose and two anonymous reviewers for their constructive criticisms that helped us improve early versions of this article.

References

Aracena, C., Lange, C.B., Iriarte, J.L., Rebolledo, L., Pantoja, S., 2011. Latitudinal patterns of export production recorded in surface sediments of the Chilean Patagonian fjords (41–55°S) as a response to water column productivity. Continental Shelf Research 31 (3–4), 340–355.

Aysen_SEIA, 2012. Proyecto Hidroeléctrico Aysén. Adenda No. 2. Available from: http://seia.sea.gob.cl/documentos/documento.php?idDocumento=5022383 (accessed 04.04.12).

Barron, M.G., Barron, K.J., 2005. Glacial influences on solar radiation in a subarctic sea. Photochemistry and Photobiology 81, 187–189.

Boyd, B.L., Anderson, J.B., Wellner, J.S., Fernández, R.A., 2008. The sedimentary record of glacial retreat, marinelly fjord, Patagonia: regional correlations and climate ties. Marine Geology 255, 165–178.

Braunschweig, F., Leitao, P.C., Fernandes, L., Pina, P., Neves, R.J.J., 2004. The object-oriented design of the integrated water modelling system MOHID. In: Proceedings of the XV International Conference on Computational Methods in Water Resources, vol. 2, pp. 1079–1090.

Campuzano, F.J., Leitão, P.C., Gonçalves, M.I., Marín, V., Tironi, A., 2008a. In: Neves, R., Baretta, J.W., Mateus, M. (Eds.), Hydrodynamical Vertical 2D Model for the Aysén Fjord. IST Press, Lisboa, Portugal, pp. 555–566.

Campuzano, F.J., Marín, V., Tironi, A., Chambel-Leitão, P., 2008b. In: Neves, R., Baretta, J.W., Mateus, M. (Eds.), Ecological Conceptual Model for a Southern Chilean Fjord: The Aysén Fjord Case Study. IST Press, Lisboa, Portugal, pp. 567–579.

Casassa, G., Wendt, J., Wendt, A., López, P., Schuler, T., H-gerd, Maas, 2010. Outburst floods of glacial lakes in Patagonia: is there an increasing trend? Geophysical Research Abstracts 12, 12821.

Chippada, S., Dawson, C., Wheeler, M., 1998. Agodonov-type finite volume method for the system of shallow water equations. Computer Methods in Applied Mechanics and Engineering 151, 105–130.

Clarke, G., Leverington, D., Teller, J., Dyke, A., 2003. Paleoclimate. Superlakes, megafloods, and abrupt climate change. Science 301, 922–923.

Costasur, 2009. Estudio Oceanográfico Oceanografía física y biológica sistema estuarino ríos Baker y Pascua, XI Región. Costasur Consultores, Chile, p. 55.

Dussaillant, A., Benito, G., Buytaert, W., Carling, P., Meier, C., Espinoza, F., 2009. Repeated glacial-lake outburst floods in Patagonia: an increasing hazard? Natural Hazards 54, 469–481.

Ghimire, M., 2005. Review of studies on glacier lake outburst floods and associated vulnerability in the Himalayas. The Himalayan Review 35/36, 49–64.

González, H.E., Castro, L., Daneri, G., Iriarte, J.L., Silva, N., Vargas, C., Giesecke, R., Sánchez, N., 2011. Seasonal plankton variability in Chilean Patagonia fjords: carbon flow through the pelagic food web of the Aysen fjord and plankton dynamics in the Moraleda Channel basin. Continental Shelf Research 31, 225–243.

Gustafsson, K.E., Bendtsen, J., 2007. Elucidating the dynamics and mixing agents of a shallow fjord through age tracer modelling. Estuarine, Coastal and Shelf Science 74, 641–654.

Huisman, J., van Oostveen, P., Weissing, F.J., 1999. Critical depth and critical turbulence: two different mechanisms for the development of phytoplankton blooms. Limnology and Oceanography 44, 1781–1787.

HydroAysén, 2010. Description of the Project. Available from: http://www.hidroaysen.cl/site/ingles/descripcion_pha.html (accessed 18.07.10).

Iriarte, J.L., González, H.E., Liu, K.K., Rivas, C., Valenzuela, C., 2007. Spatial and temporal variability of chlorophyll and primary productivity in surface waters of southern Chile (41.5–43.8 S). Estuarine, Coastal and Shelf Science 74, 471–480.

Keilegavlen, E., Bertnsen, J., 2009. Non-hydrostatic pressure in σ-coordinate ocean models. Ocean Modelling 28, 240–249.

Kirk, J.T.O., 1994. Light and Photosynthesis in Aquatic Ecosystems, Second ed. Cambridge, Great Britain, Cambridge University Press, Cambridge, UK.

Leonov, D., Kawase, M., 2009. Sill dynamics and fjord deep water renewal: idealized modeling study. Continental Shelf Research 29, 221–233.

Lopez, P., Chevallier, P., Favier, V., Pouyaud, B., Ordenes, F., Oerlemans, J., 2010. A regional view of fluctuations in glacier length in southern South America. Global and Planetary Change 71, 85–108.

Lyard, F., Lefevre, F., Letellier, T., Francis, O., 2006. Modelling the global ocean tides: modern insights from FES2004. Ocean Dynamics 56, 394L 415.

Margalef, R., 1978. Life forms of phytoplankton as survival alternatives in an unstable environment. Oceanologica Acta 1, 493–509.

Marín, V.H., Campuzano, F.J., 2008. Un modelo hidrodinámico-barotrópico para los fiordos australes de Chile entre los 41°S y los 46°S. Ciencia y Tecnología del Mar 31, 125–136.

Marín, V.H., Delgado, L.E., Tironi, A., 2008. In: Neves, R., Baretta, J.W., Mateus, M. (Eds.), The Aysén Fjord Tsunami of April 2007: Unexpected Uses of Circulation Models. IST Press, Lisboa, Portugal, pp. 597–601.

Marin, V.H., Tironi, A., Delgado, L.E., Contreras, M., Novoa, F., Torres-Gomez, M., Garreaud, R., Vila, I., Serey, I., 2009. On the sudden disappearance of *Egeria densa* from a Ramsar wetland site of Southern Chile: a climatic event trigger model. Ecological Modelling 220, 1752–1763.

Martins, F., Leitão, P.C., Silva, A., Neves, R., 2001. 3D modelling of the Sado Estuary using a new generic vertical discretization approach. Oceanologica Acta 24, 51–62.

McCarthy, J.J., Canziani, O.F., Leary, N.A., Dokken, D.J., White, K.S., 2001. Climate Change 2001. Cambridge University Press, Cambridge, UK.

Mitchell, S.B., Burgess, H.M., Pope, D.J., Theodoridou, A., 2008. Field studies of velocity, salinity and suspended solids concentration in a shallow tidal channel near tidal flap gates. Estuarine, Coastal and Shelf Science 78, 385–395.

Montecino, V., Pizarro, G., 2008. Primary productivity, biomass, and phytoplankton size in the austral Chilean channels and fjords: spring–summer patterns. In: Silva, N., Palma, S. (Eds.), Progress in the Oceanographic Knowledge of Chilean Interior Water, from Puerto Montt to Cape Horn. Comité Oceanográfico Nacional-Pontificia Universidad Católica de Valparaíso, pp. 93–97.

Neves, R., Baretta, J., Mateus, M., 2008. Perspectives on Integrated Coastal Zone Management in South America. IST Press, Lisbon, Portugal.

Ng, F., Liu, S., Mavlyudov, B., Wang, Y., 2007. Climatic control on the peak discharge of glacier outburst floods. Geophysical Research Letters 34, L21503.

Nyholm, N., Nielsen, T.K., Pedersen, K., 1984. Modeling heavy metals transport in an artic fjord system polluted from mine tailings. Ecological Modelling 22, 285–329.

Old, G.H., Lawler, D.M., Snorrason, Á., 2005. Discharge and suspended sediment dynamics during two jökulhlaups in the Skaftá river, Iceland. Earth Surface Processes and Landforms 30, 1441–1460.

Paredes, M.A., Montecino, V., 2011. Size diversity as an expression of phytoplankton community structure and the identification of its patterns on the scale of fjords and channels. Continental Shelf Research 31, 272–281.

Partheniades, E., 1965. Erosion and deposition of cohesive soils. Journal of Hydraulics Divisions, ASCE 91, 105–139.

Parsons, T.R., Takahashi, M., Hargrave, B., 1984. Biological Oceanographic Processes. Oxford.

Pickard, G.L., 1971. Some physical oceanographic features of inlets of Chile. Journal of Fisheries Research Board of Canada 28, 1077–1106.

Pizarro, G., Montecino, V., Guzmán, L., Muñoz, V., Chacón, V., Pacheco, H., Frangópulos, M., Retamal, L., Alarcón, C., 2005. Patrones locales recurrentes del fitoplancton en fiordos y canales australes (43°–56°S) en primavera y verano. Ciencia y Tecnología del Mar 28, 63–83.

Portela, L., 1996. Modelação matemática de procesos hidrodinámicos e de qualidade da agua no Estuário do Tejo. In: Dissertação para obtenção do grau de Doutor em engenharia do Ambiente. Instituto Superior Técnico, Universidade Técnica de Lisboa, p. 240.

Prado-Fiedler, R., 2009. Winter and summer distribution of dissolved oxygen, pH and nutrients at the heads of fjords in Chilean Patagonia with possible phosphorus limitation. Revista de Biología Marina y Oceanografía 44, 783–789.

Reynolds, C.S., 1997. Vegetation Processes in the Pelagic: A Model for Ecosystem Theory. Ecology Institute, Oldendorf/Luhe, p. 371.

Robins, P.E., Elliot, A.J., 2009. The internal tide of the Gareloch, a Scottish fjord. Estuarine, Coastal and Shelf Science 81, 130–142.

Silva, N., Guzmán, D., 2006. Condiciones oceanográficas físicas y químicas, entre Boca del Guafo y Fiordo Aysén (Crucero CIMAR 7 Fiordos). Ciencia y Tecnología del Mar 29, 25–44.

Silva, N., Vargas, C.A., Prego, R., 2011. Land-ocean distribution of allochtonous organic matter in surface sediments of the Chiloé and Aysén interior seas (Chilean Northern Patagonia). Continental Shelf Research 31, 330–339.

Tironi, A., Marín, V.H., Campuzano, F.J., 2010. A management tool for assessing aquaculture environmental impacts in Chilean Patagonian fjords: integrating hydrodynamic and pellets dispersion models. Environmental Management 45, 953–962.

Vargas, C.A., Martinez, R.A., San Martin, V., Aguayo, M., Silva, N., Torres, R., 2011. Allochthonous subsidies of organic matter across a lake-river-fjord landscape in the Chilean Patagonia: implications for marine zooplankton in inner fjord areas. Continental Shelf Research 31, 187–201.

Zajączkowski, M., Wlodarska-Kowalczuk, M., 2007. Dynamic sedimentary environments of an Arctic glacier-fed river estuary (Adventfjorden, Svalbard). I. Flux, deposition, and sediment dynamics. Estuarine Coastal and Shelf Science 74, 285–296.